An Inter-loop Approach on Hydrothermal Carbonization of Sewage Sludge for the Production of Biochar and Its Application as an Adsorbent for Lead-acid Battery Recycling

Vinícius Mateus Silveira Martins
Universidade Tecnologica Federal do Parana
Luiz Guilherme Giannina Sante
Universidade Tecnologica Federal do Parana
Renata Mello Giona
Universidade Tecnologica Federal do Parana
Gustavo Rafael Collere Possetti
Sanepar
Alesandro Bail (alebail@utfpr.edu.br)
Universidade Tecnológica Federal do Paraná https://orcid.org/0000-0002-1631-9302

Research Article

Keywords: hydrothermal carbonization, sewage sludge, spent sulfuric acid, circular economy, biochar

Posted Date: October 18th, 2021

DOI: https://doi.org/10.21203/rs.3.rs-960177/v1

Abstract

This work presents an inter-loop approach in which the hydrothermal carbonization (HTC) of sewage sludge allows the production of biochars capable of removing iron ions, which usually harm the lead-acid batteries performance, from spent sulfuric acid without any activation step. The HTC process was performed at three different water/biomass ratios under 180 ºC by 24 h, and except for water, no additional chemical input was used. The moisture content of the sludges ranged from 76 to 91 wt.%. Biochars were characterized by XRD, FTIR, SEM, TGA and N_2 adsorption-desorption. Results suggest a high dependence of their textural and surface properties on the water amount inside the reactor vessel. The expressive presence of multiple mineral phases in the sewage sludge allowed the formation of a hydrophilic surface, which was fundamental for the iron ions adsorption at strong acidic conditions. Porosity was strongly influenced by the water/biomass ratio, with biochar's surface displaying pore dimensions in nano and micro domains. Furthermore, the non-activated biochar presented an adsorption capacity up to 148 mgFe g^{-1}, whereas the commercial activated carbon "as received" achieved 178 mgFe g^{-1}. Results show the potential of the HTC technique for sewage sludge conversion into biochar without pre-drying, and the possibility of interconnecting two or more industrial processes in order to make them cleaner and more sustainable, matching the principles of circular economy.

1. Introduction

The generation of waste from urban and industrial activities has achieved unsustainable levels, occupying an important place in the planning of cities, as well as in managing industrial processes (Belaud et al., 2019). Therefore, the development of closed-loop technologies has emerged as a contemporary way to convert trash into treasure, even though there are cultural barriers to be overcome (Russo et al., 2019).

For instance, proposing useful applications for the sludge produced in sewage and water treatment plants is one of the hardest tasks for public managers. For comparative purposes, it is estimated that the United States produces more than 6.5 million metric tonnes of sewage sludge per year (Venkatesan et al., 2015), whereas in Brazil, where only around 59% of municipal solid waste is appropriately disposed of in sanitary landfills, the production can achieve up to 3.0 million tonnes per year (Alfaia et al., 2017; ANA, 2017). This kind of biowaste is usually discarded in landfills, causing a high environmental impact not only because of the large production worldwide but also for being considered a hazardous material due to its metal and pathogenic microorganisms' content (Jafari and Botte, 2021). Additionally, unless the distance to be covered for sewage sludge disposal exceeds a certain limit, the relatively low cost of fee taxes has discouraged the implementation of cleaner and more profitable technologies (Tesfamariam et al., 2020).

Fortunately, several alternative strategies have been proposed in order to mitigate the environmental impact of sewage sludge as well as explore its continuous and growing production, such as its

conversion into biofertilizers and its use as a source of bioenergy, two sustainable applications that have gained ground in the world scenario (Ding et al., 2016; Zaharioiu et al., 2021).

Concurrently, an industrial waste which has attracted the attention of managers is the one from lead-acid batteries. Despite the well-established lead-acid batteries recycling technologies, a recent study highlights that, unlike lead and plastic casings, the electrolyte sulfuric acid, which corresponds to up to 44 wt.% of the electrolytic cell, finds a limited route when being converted into $CaSO_4$ or Na_2SO_4 (Ballantyne et al., 2018). The spent sulfuric acid (SSA) presents a concentration ranging from 10 to 25 wt.%, demanding a large amount of base to be neutralized, as well as several heavy metals, such as Fe, Zn, Cd, Sb and Pb (Zhao et al., 2021). The multiple-valence iron is considered to generate fatal effects to the battery capacity, leading to corrosion of the electrodes, which in turn causes loss of active materials, as well as promotes selective discharge, undesirably releasing O_2 and H_2 gases. The resulting effect of iron contamination can be understood as a decrease in the battery life cycle (Lam et al., 2021; Liu et al., 2011).

In view of the foregoing, some technologies have been evaluated in order to remove iron ions from SSA aiming at enhancing the lead battery recycling process. Qifeng et al. (2016) reported a successful method based on solvent extraction followed by stripping in which the selectivity for iron(III) achieved 99.9%. Despite the excellent result, the employed method requires the use of an organic solvent as the extraction agent, which may be characterized by a critical shortcoming for industrial application, and a stage with high potential for the generation of new environmental liabilities.

Alternatively, solid-liquid adsorption is considered a powerful technique for the removal of chemical species from solution. However, the strong acid medium of the SSA demands a high chemical stability on the part of the solid adsorbent, since the drastic conditions favor its dissolution. For instance, among the adsorbents largely used in industry, zeolites show a vulnerable chemical structure, susceptible to dissolution in extreme pH conditions (Ennaert et al., 2016; Hartman and Fogler, 2007). This is an important disadvantage and makes the use of zeolites for direct SSA purification unfeasible, mainly for type A zeolites, which have a Si:Al ratio of 1 and present interconnected cavities, a material highly susceptible to dissolution in strong acidic medium (Julbe and Drobek, 2016).

On the other hand, carbon-based materials present a superior chemical stability, given the extremely drastic activation conditions that an ordinary charcoal is submitted to in order to have its surface modified. Typically, such conditions include mineral acids or bases at 10-20 wt.%, followed by thermal treatment at temperatures that achieve up to 400 or 500 ºC (Seo-Hyun et al. 2016).

In regard to carbon-based material production, pyrolysis is the most common method employed. Although pyrolysis is a well-known technology for the conversion of biomass into charcoal, the inert atmosphere, high temperature, and numerous other factors are significant disadvantages, depending on the specific type of route chosen, e.g. fixed or fluidized bed (Lopez et al., 2017).

Hydrothermal carbonization (HTC) emerges as an alternative technology to pyrolysis, mainly due to the milder experimental conditions required for biomass conversion. HTC is a thermochemical-based technique capable of converting biomass into solid, liquid and gas phases without the need for its pre-drying, which provides an interesting advantage in energetic terms (Niinipuu et al., 2020). Product distribution fundamentally depends on the type of feedstock and the temperature of the process (usually set to 180-250°C). However, there is also dependence on the reaction time and on the water:biomass ratio (Nizamuddin et al. 2017).

Also, HTC does not require any inert atmosphere to take place, since the mechanism of the process contemplates hydrolysis of the cellulose, decomposition of the hemicellulose, dehydroxylation, decarboxylation and dehydration reactions practically insensitive to the presence of O_2 (Bevan et al., 2020). Usually, sources of biomass rich in lignocellulose are widely employed in the HTC process, however, sewage sludge has been considered as a welcome feedstock because of its usually high content of water. Several works have reported the conversion of sewage sludge into hydrochars, also named biochars due to its environmental appeal (Bolognesi et al., 2021; Chen et al., 2020). Additionally, the compositional heterogeneity displayed by sewage sludges, such as the blend of organic and mineral materials may favor the formation of biochars with more appropriate surfaces to be employed in sorption processes.

The inter-loop concept represents several approaches extensively explored in the context of the circular economy by the global industry with regard to feeding one process by using tailings from another, similar to the open-loop strategy present in the well-established reuse of blast slag from steel melting furnaces as an additive for Portland cement production (Tsakiridis et al., 2008), and numerous proposals reported in the literature which involve a myriad of possibilities (Gadipelly et al., 2014; Han et al., 2021). However, these methods usually do not predict a continuous reuse of such tailings in order to create interconnected new loops, which would purposefully develop and strengthen other industrial processes.

This work reports an approach involving a first recycling process, characterized by the hydrothermal carbonization of a biowaste into a valuable material, in order to apply it in a second recycling process, related to the reuse of spent sulfuric acid from lead-acid batteries, aiming at synergism between the two processes.

2. Materials And Methods

2.1. Chemicals

A standard 1000 mg L^{-1} iron(III) solution containing 5.0% (vol/vol) nitric acid was purchased from Spetrosol; potassium thiocyanate ACS grade (KCNS) was purchased from Reagen; nitric acid (HNO_3) was purchased from Synth. Activated carbon was purchased from Quimidrol (grain size smaller than 325 Mesh, 50-70 wt.%) and was used as received.

2.2. Sampling and physico-chemical characterization of the sludges

The sludge samples were provided by the local company in charge of managing the environmental sanitation in the state of Paraná. First, the centrifuged sludge produced in the water treatment station was sampled and labeled CWS. Then, two more samples were collected in the sewage treatment station, one dehydrated (DSS) and another one pre-treated by lime (LSS). The three samples were packaged in polypropylene flasks and stored at 4°C.

The samples were submitted to gravimetric assays in order to determine their moisture and organic matter contents at 110 and 550°C, respectively. Samples were thermally treated in crucibles until they reached a constant weight.

2.3. Hydrothermal carbonization experiments

For hydrothermal treatment only the wet DSS sample was considered. Approximately 5.00 g of DSS were placed in a 40-mL stainless steel jacketed teflon vessel, followed by water addition in three different volumes: 15, 25 and 35 mL in order to achieve a water:biomass ratio (W/B) equal to 3.3, 5.3 and 7.3. The moisture water of the DSS sample was considered in the calculations. The DSS-containing stainless steel reactor was placed into an oven at 180°C for 24 or 48 h. Upon the thermal treatment, the flask was cooled at room temperature and the content was separated into liquid and solid phases by centrifugation at 4,000 RPM. The black powders of biochar were washed by distilled water and dried at 110°C overnight. For practicality, the dried samples were labeled BC3, BC5 and BC7, according to the W/B ratio used in the experiments.

2.4. Characterization post-hydrothermal carbonization

Transmission Fourier Transform Infrared (FTIR) spectra were registered on a Perkin Elmer FTIR spectrometer model Frontier in the range 400-4000 cm^{-1}, using KBr pellets. KBr was ground with a small amount of the solid to be analyzed, and the spectra were collected with a resolution of 4 cm^{-1} and an accumulation of 32 scans.

Powder X-ray diffraction analysis (PXRD) was conducted in a Bruker D2 Phaser diffractometer operating at 30 kV and 10 mA with copper radiation (Cu-K_a=0.15418 nm) in the range 7-80 ° with dwell time of 2 °/min.

Scanning electron microscopy (SEM) was recorded in a FE-SEM (TESCAN, model MIRA 3 LMU, Brno, Kohoutovice, Czech Republic). Around 10 mg of sample was dispersed in 1 mL of water and one drop of the suspension was placed in the sample holder in order to evaporate the solvent at 30°C for 10 min.

N_2 adsorption/desorption analysis was performed in order to measure the specific surface area, the average pore diameter and the pore volume of the biochars. For this purpose, the BET (Brunauer et al., 1938) and the BJH (Barrett et al. 1951) methods were applied to the corresponding nitrogen adsorption

isotherms, which were collected on an ASAP 2020 N Automatic Physisorption Analyzer from Micrometrics at 77 K. The samples were previously degassed by treatment at 120 ºC until the system pressure achieved 10 µmHg. The nitrogen adsorption data were obtained by using approximately 0.1 g of the sample.

Thermogravimetric analysis (TGA) included TG and DSC experiments. They were simultaneously performed on a Perkin Elmer 195 thermal analyzer model STA 6000, where approximately 10 mg of the sample was placed in an open platinum crucible and pre-heated at 100°C for 5 min. The experiments were carried out in a N_2 atmosphere, at a flow rate of 10 mL min^{-1} and a heating rate of 10°C min^{-1}, in the range 50-650°C.

Electronic absorption spectra (UV-Vis) in solution were obtained on a single-beam Biochrom UV-Vis spectrometer model S60 Libra, in the range 400-800 nm.

2.5. Adsorption experiments

For the adsorption experiments, 30 mL of an Fe(III) stock aqueous solution, prepared by the mixture of an aliquot of a 1000 mg L^{-1} standard solution and H_2SO_4 98.0 wt.% diluted with distilled water, was transferred to a 125-mL propylene flask. Then, a weight of the biochar BC5 or CAC was added to generate iron(III):adsorbent ratio (Fe:ADS) ranging from 30 to 300 in weight. The reaction flasks were incubated in an orbital shaker at 180 rpm, 30°C for 30 min. Upon vigorous contact, the content was transferred to conical flasks and centrifuged at 4000 rpm for 3 min each. The supernatant was mixed to a 2.0x10^{-3} mol L^{-1} KCNS aqueous solution with a constant HNO_3 acidity of 5.0%. Then, the resulting $[Fe(NCS)(OH_2)_5]^{2+}$ reddish complex was analyzed by UV-Vis spectroscopy at λ_{max} = 460 nm. The maximum adsorption at equilibrium (q_e) was calculated according to Equation 1:

$$q_e = \frac{(C_0 - C_1)V}{m}$$

1

where:

q_e = maximum adsorption capacity (mg g^{-1});

C_o = iron(III) initial concentration (mgFe L^{-1});

C_i = iron(III) concentration at equilibrium (mgFe L^{-1})

V = volume of acidic iron(III) solution (L)

m = mass of adsorbent (g)

3. Results And Discussion

3.1. Moisture and organic contents of the sludges

The sludges were submitted to gravimetric analysis in order to evaluate their moisture and organic contents, a relevant information to drive the HTC tests. Fig. 1 shows CWS, DSS and LSS samples, as well as the results obtained from the gravimetric tests. Organic matter content was expressed in wet base. The sum of moisture, organic matter and ash contents results in 100 wt.% of the sewage sludge composition.

The CWS sample had a paste-like appearance, which is in agreement with its higher moisture content (78.5 wt.%). On the other hand, it presented the lowest organic matter content (4.4 wt.%), which would not favor the HTC tests. The DSS sample presented moisture and organic matter contents of 29.5 and 35.2 wt%., respectively. Its higher organic matter content was responsible for the choice of this sample as the most suitable for the HTC tests. In its turn, the LSS sample was disregarded for the HTC tests due to its lower organic matter content (25.3 wt.%) and the presence of lime, which could interfere in the carbonization process and would not match the scope of this work.

3.2. Performance in the HTC tests

Two different phases were observed at the end of the HTC experiments: a liquid formed by the bio-oil and a solid formed by the biochar (Fig. 2). The mass yield was studied by the variation of time and W/B ratio. Fig. 2 shows the mass yields obtained for W/B = 3.3, 5.3 and 7.3 over 24 or 48 h.

For all the tests, the obtained biochar yield ranged from 30 and 50 wt.%. In general, shorter reaction time led to higher weight of biochar, whereas the W/B ratio did not significantly influence the biochar yield. The results are in agreement with the organic matter content of the DSS sample (48.9 wt.%) and suggest that the organic matter content is essential to enable the use of this kind of sludge as a precursor of biochar. The W/B ratio range covered by the experiments can be expressed as a percentage of moisture, ranging from 76 to 91 wt.%, which allows us to confirm the feasibility of the HTC process under real operating conditions of a sewage treatment plant (Wilk et al., 2021). In addition, such moisture content usually makes the sludge more fluid, like a loose paste, which can favor aspects of transfer by pumping and avoid costs related to its preparatory dehydration.

3.3. Characterization of the biochars

FTIR spectra obtained for the biochars are presented in Fig. 3. The three biochars showed a similar profile with a series of absorption bands in the evaluated range. In general, the bands are in agreement with the previously reported in the literature (Lu et al., 2017). The broad band centered at 3300 cm^{-1} in Fig. 3a was attributed to H_2O and OH stretching modes, as well as the band at 1612 cm^{-1} was attributed to H_2O bending mode. These strong vibrational modes indicate that the biochar surface is predominatly formed by polar groups (Bernardino et al., 2016), which may favor sorption processes involving metal ions. The bands at 759 and 1010 cm^{-1} were attributed to siloxane (Si-O-Si) stretching modes, confirming the presence of SiO_2, which is in agreement with the ash content of DSS. In addition, the presence of inorganic compounds could also be confirmed by the two bands around 542 cm^{-1}, referring to metal-

oxygen (M-O) stretching modes, provenient, for instance, from the typically abundant iron and aluminum metals. Moreover, the biochars were further characterized with regard to the organic part of their composition. The presence of hydrocarbons was confirmed by the two bands at around 2879 cm^{-1}, attributed to the stretching modes of terminal CH_3 groups, as well as the bending modes of CH_2 groups at around 1340 cm^{-1}. The presence of amide (CONH) and carbonyl (C=O) groups was suggested by the bands centered at 1515 and 1735 cm^{-1}. In its turn, the band at 1150 cm^{-1} was attributed to C-O-C glycosidic bounds, which suggests the presence of non-converted oligosaccharide or triacylglycerol compounds (Fang et al., 2019). In Fig. 3b, it is possible to confirm the presence of SiO_2 due to the band centered at 910 cm^{-1}, attached to the silanol (Si-OH) stretching mode. Also, Fig. 3b shows a sharp band at around 3700 cm^{-1}, which is usually attributed to the presence of free H_2O molecules (Lengyel et al., 2017), probably associated with a more hydrophilic surface, richer in silanol groups.

Figure 4 depicts the PXRD for the synthesized biochars. The set of diffraction peaks for the three biochars confirmed the existence of a mixture of inorganic and organic compounds. The presence of carbonaceous compounds could be characterized by the narrow and sharp graphite peak at 26.8° (2θ). Literature reports that a biochar typically has an amorphous PXRD profile (Uchimiya et al., 2017), however, several crystalline phases can be identified in Fig. 4a, such as halloysite at 2θ = 9.6° (Li et al., 2017), kaolinite at 2θ = 20.5, 25.2 and 50.2° (Meroufel et al., 2013), quartz at 2θ = 21.1, 27.7 and 68.1º (Tavares et al., 2020), and alumina (α + γ polymorphs) at 2θ = 35.9 and 54.6° (Chauruka et al., 2015). Fig. 4b shows an additional diffraction peak at 43.2° (2θ), which was attributed to γ-alumina, and Fig. 4c shows the additional diffraction peak centered at 28.9° (2θ), attributed to calcium carbonate (Ranjan et al., 2018), which may have been formed by a leaching process, intensified by the high W/B, resulting in a higher availability of calcium ions. Anyhow, the presence of a large amount of crystalline compounds may strongly influence the strength of sorption sites and acid-base surface properties of the material.

SEM images show that the variation in the W/B ratio plays an important role on the biochar porosity (Fig. 5). The lowest W/B ratio favored the formation of micrometric pores, apparently achieving an average of 4 µm, with smaller channels on the inside (Fig. 5a-c). As the W/B was increased, the porosity of the biochar was decreased. BC5 presented smaller pores around 100 nm (Fig. 5d-f), and BC7 did not present visible pores in the SEM images (Fig. 5g-i). The BC5 images depict a clear presence of graphite sheets, highly organized and containing nanometric pores.

Another important consideration is the clear modification of the textural profile of the biochars after the HTC process. The lower W/B ratio (Fig. 5a-c) allowed an increase in the conversion of the smooth sheets into porous structures, similarly to what was reported for high temperature pyrolysis processes (Khosravi et al., 2019).

The mineral phases can also be seen in the images, such as angular-shaped quartz agglomerates and rod-shaped halloysite (Li et al., 2015) embedded in the graphite sheets and quartz crystallites (Fig. 5e and 5h).

Considering the characteristics of the formed surfaces, it can be highlighted that the W/B ratio strongly influenced the hydrocarbonization of the DSS. Besides the water availability, the inner pressure of the hermetic system may have been a crucial factor in the decarboxylation and polymerization reactions, promoting an increase of the DSS hydrocarbonization. Literature clearly reports the dependence of the HTC process on the W/B ratio (Ischia and Fiori, 2021), focusing mainly on the reaction yield. However, there is a lack of discussion on the influence of the W/B ratio over the morphology of the hydrochars.

The nitrogen physisorption isotherms are depicted in Fig. 6. The biochars presented a Type III isotherm loop, typically of nonporous or macroporous materials (ALOthman, 2012). Based on the SEM images (Fig. 5), the non-porosite of the biochars was disregarded, emphasizing instead the domain of large pores in the micrometric range (BC3) and high order nanopores (above 100 nm) in the case of BC5. BC7 showed a similar isotherm profile, however, it was not possible to establish a direct relation with the SEM images. In addition, the hysteresis loop in the range 0.7-1.0 P/P_0 was observed for the three synthesized biochars and attached to the H3 type, typically due to the existence of mesopores (Yin et al., 2015). Therefore, the biochars presented a large heterogeneity of its pore size, drawing attention to further exploring studies on hierarchically structured porous materials (Leżańska et al., 2018). Additionally, as a direct result of the large pore size distribution, the BET method took into account only a small range of mesopores, resulting in the subestimated values of surface specific area (around 6 $m^2\ g^{-1}$), and a discrete pore volume (ranging from 0.02 to 0.05 $cm^3\ g^{-1}$) (Table 1).

Table 1
N_2 adsorption/desortpion results.

ID	Specific area ($m^2\ g^{-1}$) [a]	Average pore size (nm) [b]	Pore volume ($cm^3\ g^{-1}$) [b]
BC3	6.3	16.6	0.05
BC5	6.5	1.32	0.04
BC7	5.9	7.44	0.02

[a] Determined by N_2 adsorption using the Brunauer-Emmett-Teller (BET) method.

[b] Determined by the N_2 desorption branch using the Barret-Joiner-Halenda (BJH) method.

TG and DSC experiments were performed to evaluate the thermal stability of the biochars upon hydrothermal carbonization, whose main results are shown in Fig. 7. Owing to the applied experimental conditions (heating under N_2 atmosphere), the TG/DSC curves actually depict a kind of pyrolysis over the synthesized biochars. The wide endothermic curve resulting from DSC analysis was attached to an overlay of events related to the mineral and organic biochar portions, i.e. kaolinite dehydration and dehydroxylation (Wang et al., 2011) and quartz β-α polymorphs transition (Labus, 2017). Additionally,

depolymerization and decomposition involving cellulose, hemicellulose and lignin, which are remnants of the HTC process, accompanied by weight loss in the TG curve (Magdziarz et al., 2020), as well as the total decomposition of the semi-decomposed graphite present in the biochars.

Once again it is possible to notice that the W/B ratio played an important role over the synthesized biochars. BC3 and BC7 displayed a more similar profile, with the first step of weight loss centered at 250.3 and 254.8 ºC, respectively, and the second one centered at 341.3 and 435.4 ºC, respectively, referring mainly to the pyrolysis of the biochars. The highest thermal stability presented by BC7 for its second step may have been to the higher level of compaction of its grains. The total ash content for BC3 and BC7 at 640 ºC was 34.4 and 44.3 wt.%, respectively, suggesting that a higher W/B ratio can influence the material structure at the end of the HTC process.

The DSC curve for BC5 depicts a comprehensive endothermic event similar to those discussed for BC3 and BC7, showing heat flows ranging from -87 to -100 mW, respectively. On the other hand, BC5 displayed a different profile for its TG curve. Unlike for BC3 and BC7, its DTG curve (Fig. 7c) displayed the first step of weight loss at a lower temperature (134.4°C), attributed to a free water elimination process. This is in agreement with the discussion carried out on FTIR results, which pointed to a more hydrophilic surface in the case of BC5. Since the three biochars were prepared under the same experimental conditions, except W/B ratio, it is reasonable to infer that at W/B ratio of 5.3 the DSS had its hydrothermal carbonization process conditioned to a slightly slower decarboxylation and dehydration, leading to a higher capacity to incorporate water molecules. Furthermore, the lower weight loss experienced by the BC5 (around 80 wt.% at 640 ºC) reinforces the thermal stability of this material.

3.4. Adsorption experiments

BC5 was chosen as a test adsorbent for iron(III) removal from sulfuric acid aqueous solution due to its higher hydrophilicity and textural properties. For comparative purposes, commercial activated carbon (CAC) was used as a reference adsorbent. Fig. 8 shows the results obtained in the adsorption experiments.

As can be seen, the iron:adsorbent (Fe:ADS) weight ratio did not cause a significant influence on the iron(III) adsorption for both adsorbents, that is, they were capable of removing iron(III) even at high Fe:ADS ratios ranging from 200 to 300. Apparently, CAC presented a superior performance, achieving more than 80.0 wt.% of iron(III) removal in all the experiments. For BC5, the iron(III) removal was slightly lower, ranging from 70 to 80 wt.%. The best performance of the CAC yielded an adsorption capacity of 178 mgFe g^{-1}, whereas for BC5, the adsorption capacity was 143 mgFe g^{-1}. Despite the 20 wt.% difference in the adsorption capacity, it is necessary to highlight that BC5 did not undergone any activation treatment, which represents a surprising behavior. The SEM image for BC5 (Fig. 5f) shows a detail of the graphite plates arranged side by side and the abundant presence of nanopores on the surface. As is known, the BET method is not capable of detecting nanopores, resulting in an underestimated accounting of the pores actually present in the BC5 material.

Furthermore, the adsorption capacity was purposefully obtained at drastic acid conditions to simulate a batch treatment for polishing of the 15-20 wt.% spent sulfuric acid aqueous solution, containing up to 1000 mgFe L^{-1}. Even under such conditions, in which the surface of a solid adsorbent may be completely protonated (Ambaye et al., 2021), the BC5 was capable of removing up to 80 wt.% of the iron(III) content after 30 min of contact. These preliminary results show the potential of the biochar produced by the HTC process to be applied as adsorbents for the purification of spent sulfuric acid generated in the lead-acid battery sector, developing a sustainable technology for its recycling.

Further advances in this inter-loop technology consider the use of the spent biochar, rich in iron ions, as a potential surface for hydrogen sulphide removal from biogas, such that the spent H_2SO_4 polishing process could be faced as a preparatory step for that.

4. Conclusions

Biochars could be successfully produced by hydrothermal carbonization and, without any activation step, they were capable of removing iron ions from spent sulfuric acid. As the sewage sludge did not require any dehydration treatment, its use for biochar production displayed a tremendous advantage in energetic terms for sanitation companies.

Nevertheless, the water/biomass ratio plays an important role in tuning the characteristics of the biochar surface, e.g. to make it more hydrophilic and appropriate for the adsorption of metal ions. Additionally, the mineral phases may also contribute to adsorption performances, since active sites are usually dependent on the strength of the physical or chemical interactions between ions and surface. Therefore, for the adsorption of ions, the balance of organic and mineral contents of a given sludge, seems to be fundamental to form both a porous and a hydrophilic surface.

At last but not least, the inter-loop approach involving sanitation and energy sectors is a virtuous strategy to interconnecting two or more industrial processes in order to feed one through the use of tailings from another.

Declarations

Acknowledgements

We would like to acknowledge the financial support obtained from CAPES (Coordenação de Aperfeiçoamento de Pessoal de Nível Superior) and CNPq (Conselho Nacional de Desenvolvimento Científico e Tecnológico). We are also thankful for the technical support of the LabMult – the Multi-User Laboratory of UTFPR (Universidade Tecnológica Federal do Paraná). A special thanks to Sanepar (Paraná Sanitation Company) for kindly providing the samples used in this work.

Conflict of interests/competing interests

The authors declared that they have no conflicts of interest to this work.

Data availability statments

The datasets generated during and/or analysed during the current study are not publicly available due to confidentiality issues given the potential for technology development and innovation in the Brazilian industrial sector, but are available from the corresponding author on reasonable request.

References

1. Alfaia, R.G. de S. M., Costa, A. M., Campos, J. C. Municipal solid waste in Brazil: A review. Waste Manag. Res. 35 (2017) 1195–1209. https://doi.org/10.1177/0734242X17735375.
2. ALOthman, Z.A. A Review: Fundamental Aspects of Silicate Mesoporous Materials. Materials, 5 (2012) 2874–2902. https://doi.org/10.3390/ma5122874.
3. Ambaye, T.G., Vaccari, M., van Hullebusch, E.D., Amrane, A., Rtimi, S. Mechanisms and adsorption capacities of biochar for the removal of organic and inorganic pollutants from industrial wastewater. Int. J. Environ. Sci. Techenol. 18 (2021) 3273–3294. https://doi.org/10.1007/s13762-020-03060-w.
4. ANA - The Brazilian National Water Agency: Atlas sewage, pollution of watersheds 2017 (2017). http://atlasesgotos.ana.gov.br/. Accessed 16 Sep 2021.
5. Ballantyne A.D., Hallett J.P., Riley D.J., Shah N., Payne, D.J. Lead acid battery recycling for the twenty-first century. R. Soc. Open Sci. 5 (2018) 171368-171380. R. Soc. open sci.5: 171368. http://dx.doi.org/10.1098/rsos.171368.
6. Barrett, E.P., Joyner, L.G., Halenda, P.P. The determination of pore volume and area distributions in porous substances. I. Computations from nitrogen isotherms, J. Am. Chem. Soc. 73 (1951) 373–380. https://doi.org/10.1021/ja01145a126.
7. Belaud, J.-P., Adoue, C., Vialle, C., Chorro, A., Sablayrolles, C. A circular economy and industrial ecology toolbox for developing an eco-industrial park: perspectives from French policy. Clean. Technol. Environ. Policy, 21 (2019) 967–985. https://doi.org/10.1007/s10098-019-01677-1
8. Bernardino, C.A.R., Mahler, C.F., Veloso, M.C.C., Romeiro, G.A. Preparation of biochar from sugarcane by-product filter mud by slow pyrolysis and its use like adsorbent. Waste Biomass Valor. 8 (2016) 2511–2521. https://doi.org/10.1007/s12649-016-9728-5.
9. Bevan, E., Fu, J., Zheng. Y. Challenges and opportunities of hydrothermal carbonisations in the UK; case study in Chirnside. RSC Adv. 10 (2020) 31586-31610. https://doi.org/10.1039/D0RA04607H.
10. Bolognesi, S., Bernardi, G., Callegari, A., Dondi, D., Capodaglio, A.G. Biochar production from sewage sludge and microalgae mixtures: properties, sustainability and possible role in circular economy. Biomass Conv. Bioref. 11 (2021) 289–299. https://doi.org/10.1007/s13399-019-00572-5.
11. Brunauer, S., Emmett, P.H., Teller, E. Gases of gases multimolecular layers. J. Am. Chem. Soc. 60 (1938) 309–319. https://doi.org/10.1021/ja01269a023.

12. Chauruka, S.R., Hassanpour, A., Brydson, R., Roberts, K.J., Ghadiri, M., Stitt, H. Effect of mill type on the size reduction and phase transformation of gamma alumina. Chem. Eng. Sci. 134 (2015) 774–783. https://doi.org/10.1016/j.ces.2015.06.004.
13. Chen, W.-T., Haque, Md.A., Lu. T., Aierzhati, A., Reimonn. G., A perspective on hydrothermal processing of sewage sludge. Curr. Opin. Environ. Sci. Health, 14 (2020) 63-73. https://doi.org/10.1016/j.coesh.2020.02.008.
14. Ding, Y., Liu, Y., Liu, S., Li. Z., Tan, X., Huang, X., Zeng, G., Zhou, L., Zheng, B. Biochar to improve soil fertility. A review. Agron. Sustain. Dev. 36 (2016) 36-54. https://doi.org/10.1007/s13593-016-0372-z.
15. Ennaert, T., Aelst, J.V., Dijkmans, J., Clerq, R.D., Schutyser, W., Dusselier, M., Verboekend, D., Sels, B.B. Potential and challenges of zeolite chemistry in the catalytic conversion of biomass. Chem. Soc. Rev. 45 (2016) 584-611. https://doi.org/10.1039/C5CS00859J.
16. Fang, W., Dai, Y.Y., Wang, T., Gao, H.T., Huang, P., Yu. J., Huang, H.P., Wang, D.L., Zong, W.L., Aminated β-cyclodextrin-grafted Fe_3O_4-loaded gambogic acid magnetic nanoparticles: preparation, characterization, and biological evaluation. RSC Adv. 9 (2019) 27136-27146. https://doi.org/10.1039/C9RA04955J.
17. Gadipelly, C., Pérez-González, A., Yadav, G.D., Ortiz, I., Ibáñez, R., Rathod, V.K., Marathe, K.V. Pharmaceutical industry wastewater: Review of the technologies for water treatment and reuse. Ind. Eng. Chem. Res. 53 (2014) 11571–11592. https://doi.org/10.1021/ie501210j.
18. Han, N., Zhang, J., Hoang, M., Gray. S., Xie, Z. A review of process and wastewater reuse in the recycled paper industry. Environ. Technol. Innov. 24 (2021) 101860-. https://doi.org/10.1016/j.eti.2021.101860.
19. Hartman, R.L. and Fogler, H.S. Understanding the dissolution of zeolites. Langmuir, 23 (2007) 5477–5484. https://doi.org/10.1021/la063699g.
20. Ischia, G. and Fiori, L. Hydrothermal carbonization of organic waste and biomass: A review on process, reactor, and plant modeling. Waste Biomass Valor. 12 (2021) 2797–2824. https://doi.org/10.1007/s12649-020-01255-3.
21. Jafari, M., Botte, G.G. Electrochemical treatment of sewage sludge and pathogen inactivation. J. Appl. Electrochem. 51 (2021) 119–130. https://doi.org/10.1007/s10800-020-01481-6.
22. Julbe A. and Drobek M. Zeolite A Type. In: Drioli E., Giorno L. (eds) Encyclopedia of Membranes. Springer, Berlin, Heidelberg (2016). https://doi.org/10.1007/978-3-662-44324-8_604.
23. Khosravi, M., Mehrdadi, N., Nabi Bidhendi, G., Baghdadi, M. Synthesis of sewage sludge-based carbon/TiO_2/ZnO nanocomposite adsorbent for the removal of Ni(II), Cu(II), and chemical oxygen demands from aqueous solutions and industrial wastewater. Water Environ. Res. (2019) 1-16. https://doi.org/10.1002/wer.1253.
24. Labus, M. Thermal methods implementation in analysis of fine-grained rocks containing organic matter. J. Therm. Anal. Calorim. 129 (2017) 965–973. https://doi.org/10.1007/s10973-017-6259-7.
25. Lam, L.T., Ceylan, H., Haigh, N.P., Lwin, T., Rand, D.A.J. Influence of residual elements in lead on oxygen- and hydrogen-gassing rates of lead- acid batteries. J. Power Sources, 195 (2010) 4494-

4512.https://doi.org/10.1016/j.jpowsour.2009.12.020.

26. Lengyel. J., Ončák, M., Herburger, A., Linde, Christian V.D.C., Beyer, M.K. Infrared spectroscopy of $O^{\bullet}-$ and OH− in water clusters: evidence for fast interconversion between $O^{\bullet}-$ and $OH^{\bullet}OH-$. Phys. Chem. Chem. Phys. 19 (2017) 25346-25351. https://doi.org/10.1039/C7CP04577H.
27. Leżańska, M., Olejniczak, A., Łukaszewicz, J.P. Hierarchical porous carbon templated with silica spheres of a diameter of 14 nm from pure chitosan or a chitosan/$ZnCl_2$ solution. J. Porous Mat. 25 (2018) 1633–1648. https://doi.org/10.1007/s10934-018-0577-4.
28. Li, X., Ouyang, J., Zhou, Y., Yang, H. Assembling strategy to synthesize palladium modified kaolin nanocomposites with different morphologies. Sci. Rep. 5 (2015) 13763-13764. https://doi.org/10.1038/srep13763.
29. Li, Y., Zhang, Y., Zhang, Y., Zhang, Y., Liu, M., Zhang, F., Wang, L. Thermal behavior analysis of halloysite selected from Inner Mongolia Autonomous Region in China. J. Therm. Anal. Calorim. 129 (2017) 1333–1339. https://doi.org/10.1007/s10973-017-6324-2.
30. Liu, J., Yang, D., Gao, L., Zhu, X., Yang, L.L.J. Effect of iron doped lead oxide on the performance of lead acid batteries. J. Power Source. 196 (2011) 8802-8808. https://doi.org/10.1016/j.jpowsour.2011.06.084.
31. Lopez, G., Artetxe, M., Amutio, M., Bilbao, J., Olazar, M. Thermochemical routes for the valorization of waste polyolefinic plastics to produce fuels and chemicals. A review. Renew Sust Energ Rev. 73 (2017) 346-368. https://doi.org/10.1016/j.rser.2017.01.142.
32. Lu, J., Zhang, C., Wu, J., Luo, Y. Adsorptive removal of bisphenol A using N-doped biochar made of ulva prolifera. Water, Air, & Soil Pollut. 228 (2017) 327-335. https://doi.org/10.1007/s11270-017-3516-0.
33. Magdziarz, A., Wilk, M., Wądrzyk, M. Pyrolysis of hydrochar derived from biomass – Experimental investigation. Fuel, 267 (2020) 117246-117256. https://doi.org/10.1016/j.fuel.2020.117246.
34. Meroufel, B., Benali, O., Benyahia, M., Zenasni, M.A., Merlin, A., George, B. Removal of Zn (II) from aqueous solution onto kaolin by batch design. J. Water Resource Prot. 5 (2013) 669–680. https://doi.org/10.4236/jwarp.2013.57067.
35. Niinipuu, M., Latham, K.G., Boily, J.-F., Bergknut, M., Jansson, S. The impact of hydrothermal carbonization on the surface functionalities of wet waste materials for water treatment applications. Environ. Sci. Pollut. Res. 27 (2020) 24369–24379. https://doi.org/10.1007/s11356-020-08591-w.
36. Nizamuddin, S., Baloch, H.A., Griffin, G.J., Mubarak, N.M., Bhutto, A.W., Abro, R., Mazari, S.A., Ali, B.S. An overview of effect of process parameters on hydrothermal carbonization of biomass. Renew. Sustain. Energy Rev. 73 (2017) 1289–1299. http://dx.doi.org/10.1016/j.rser.2016.12.122.
37. Qifeng, W., Xiulian, R., Jingjing, G., Yongxing, C. Recovery and separation of sulfuric acid and iron from dilute acidic sulfate effluent and waste sulfuric acid by solvent extraction and stripping. J. Hazard. Mat. 304 (2016) 1–9. http://dx.doi.org/10.1016/j.jhazmat.2015.10.049.
38. Ranjan, R., Narnaware, S.D., Patil, N.V.A. Novel technique for synthesis of calcium carbonate nanoparticles. Natl. Acad. Sci. Lett. 41 (2018) 403–406. https://doi.org/10.1007/s40009-018-0704-4.

39. Russo, I., Confente, I., Scarpi, D., Hazen, B. From trash to treasure: The impact of consumer perception of bio-waste products in closed-loop supply chains. J. Clean. Prod. 218 (2019) 966-974. https://doi.org/10.1016/j.jclepro.2019.02.044.
40. Seo-Hyun, P., Jeon, M.-J., Jeon, Y.-W. Study of sulfuric acid treatment of activated carbon used to enhnce mixed VOC removal. Int. Biodeterior. Biodegrad. 113 (2016) 195-200. https://doi.org/10.1016/j.ibiod.2016.04.019.
41. Tavares, L.R.C., Tavares Junior, J.F., Costa, L.M., Bezerra, A.C.S., Cetlin, P.R., Aguilar, M.T.P. Infuence of quartz powder and silica fume on the performance of Portland cement. Sci. Rep. 10 (2020) 21461-21475. https://doi.org/10.1038/s41598-020-78567-w.
42. Tesfamariam, E. H., Ogbazghi, Z. M., Annandale, J. G., Gebrehiwot, Y. Cost–benefit analysis of municipal sludge as a low-grade nutrient source: A case study from South Africa. Sustainability, 12 (2020) 9950-9963. https://doi.org/10.3390/su12239950.
43. Tsakiridis, P.E., Papadimitriou, G.D., Tsivilis, S., Koroneos, C. Utilization of steel slag for Portland cement clinker production. J. Hazard. Mat. 152 (2008) 805–811. https://doi:10.1016/j.jhazmat.2007.07.093.
44. Uchimiya, M., Pignatello, J.J., White, J.C., Hu, S.-T., Ferreira, P.J. Structural transformation of biochar black carbon by C60 superstructure: Environmental implications. Sci. Rep. 7 (2017) 11787-. https://doi.org/10.1038/s41598-017-12117-9.
45. Venkatesan, A.K., Done, H.Y. Halden, R.U. United States National sewage sludge repository at Arizona State University—a new resource and research tool for environmental scientists, engineers, and epidemiologists. Environ. Sci. Pollut. Res. 22 (2015) 1577–1586. https://doi.org/10.1007/s11356-014-2961-1.
46. Wang, H., Li, C., Peng, Z., Zhang, S. Characterization and thermal behavior of kaolin. J. Therm. Anal. Calorim. 105 (2011) 157–160. https://doi.org/10.1007/s10973-011-1385-0.
47. Wilk, M., Śliz, M., Gajek, M. The effects of hydrothermal carbonization operating parameters on high-value hydrochar derived from beet pulp. Renew. Energy, 177 (2021) 216–228. https://doi.org/10.1016/j.renene.2021.05.112.
48. Yin, J., Song, K., Lu, Y., Zhao, G., Yin, Y. Comparison of changes in micropores and mesopores in the wood cell walls of sapwood and heartwood. Wood Sci. Technol. 49 (2015) 987–1001. https://doi.org/10.1007/s00226-015-0741-9.
49. Zaharioiu, A.M., Bucura, F., Ionete, R.E., Marin, F., Constantinescu, M., Oancea, S. Opportunities regarding the use of technologies of energy recovery from sewage sludge. SN Appl. Sci. 3 (2021) 775-786. https://doi.org/10.1007/s42452-021-04758-3.
50. Zhao, Y., Pohl, O., Bhatt, A.I., Collis, G.E., Mahon, P.J., Rüther, T., Hollenkamp, A.F. A Review on battery market trends, second-life reuse, and recycling. Sustain Chem. 2 (2021) 167-205. https://doi.org/10.3390/suschem2010011.

Figures

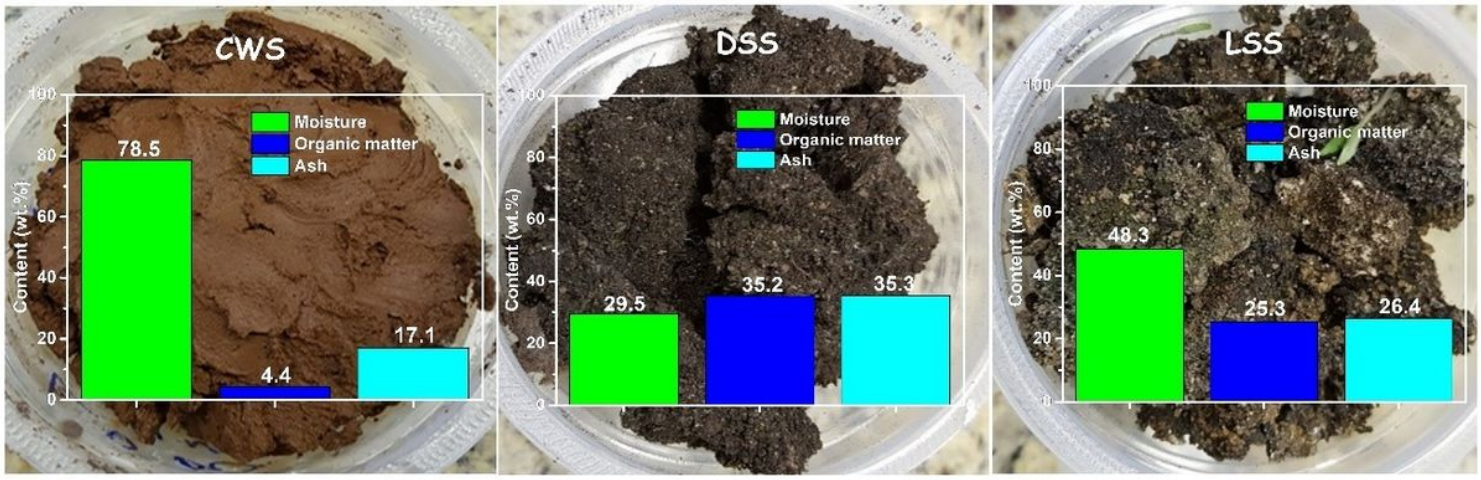

Figure 1

Appearance and moisture, organic, and ash contents of the sewage sludges studied. (Organic matter and ash are expressed in relation to the wet base).

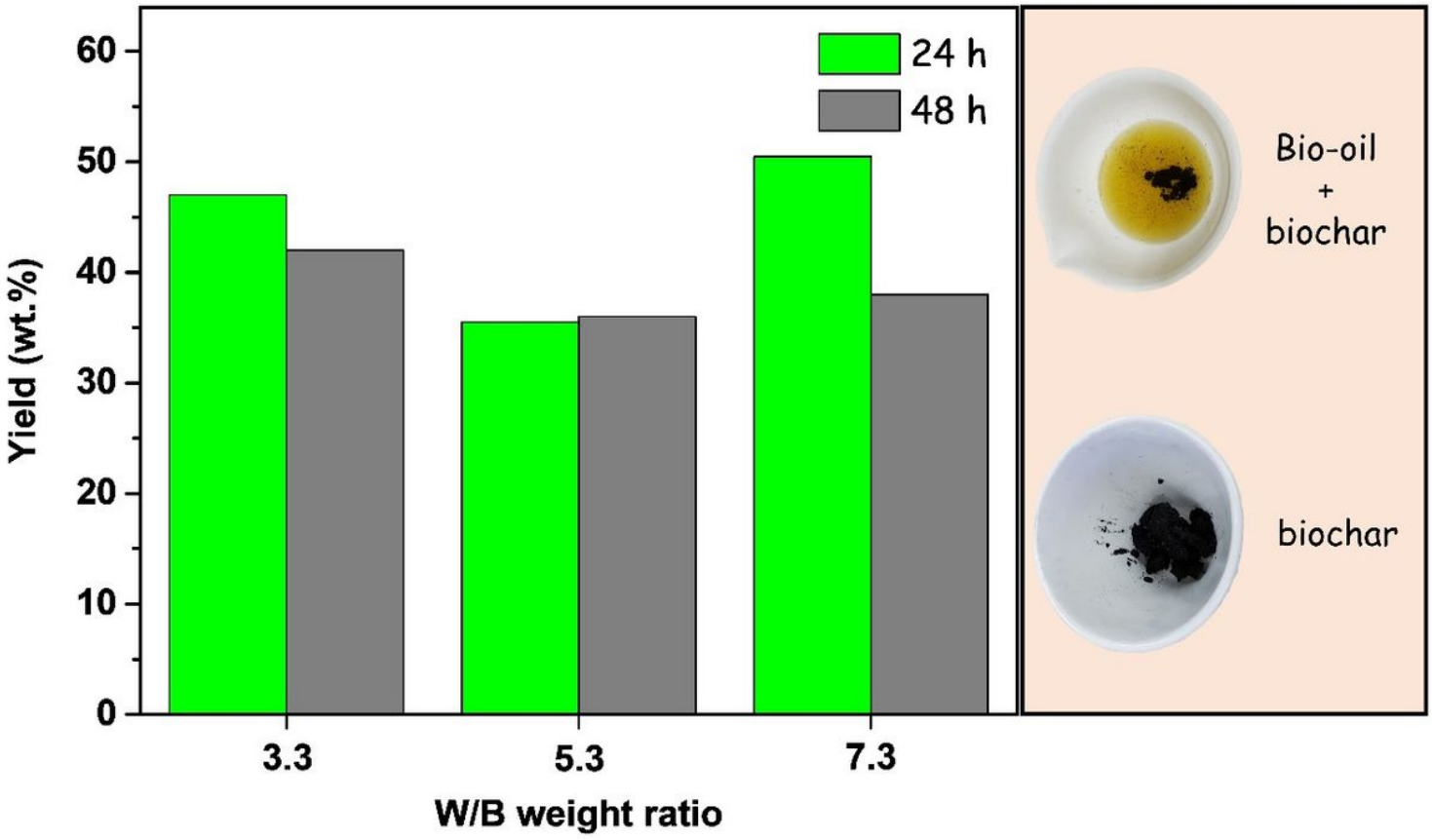

Figure 2

HTC reactions yield in three W/B ratios, and the aspect of the products formed.

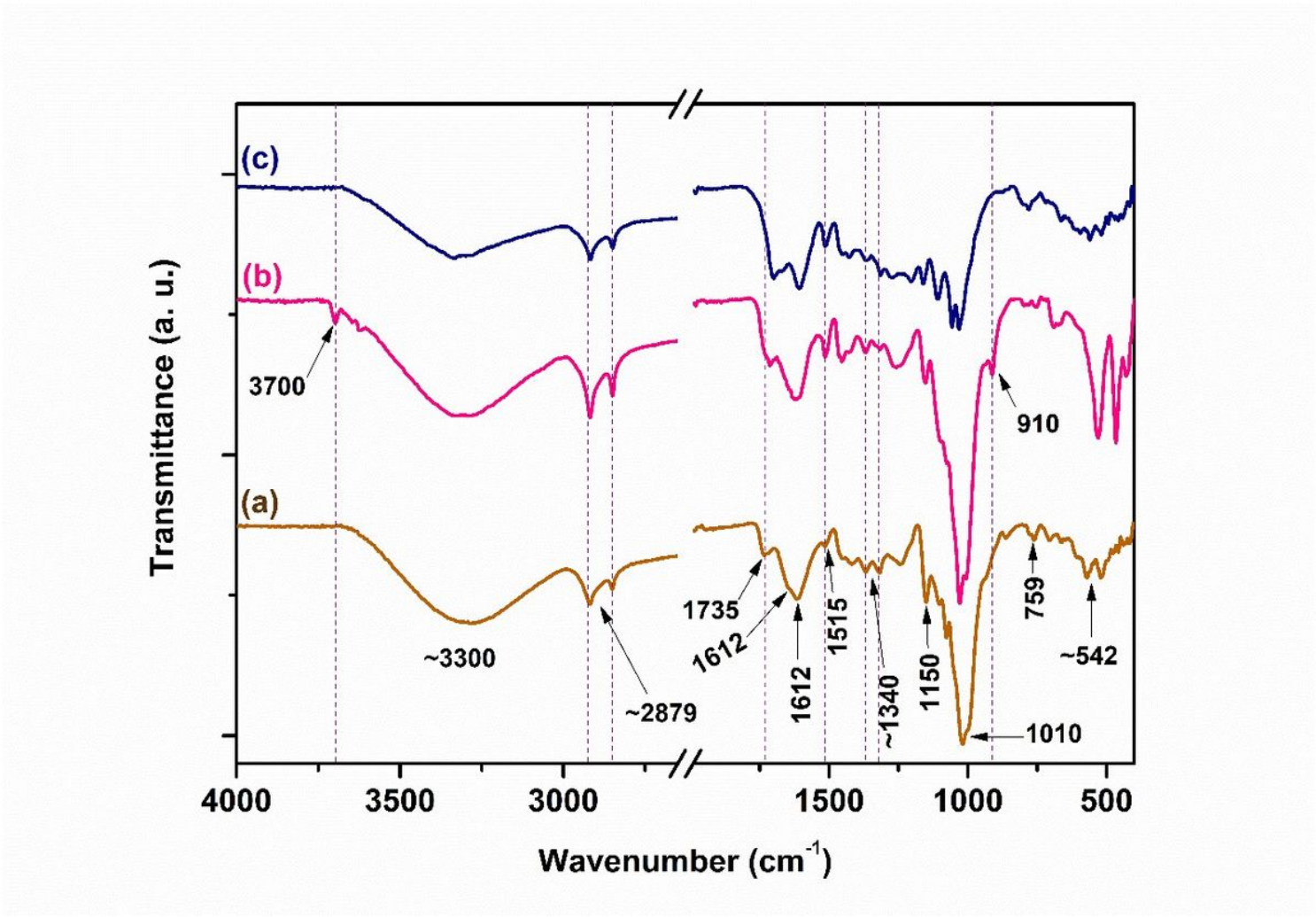

Figure 3

FTIR spectra for the synthesized biochars (a) BC3, (b) BC5 and (c) BC7.

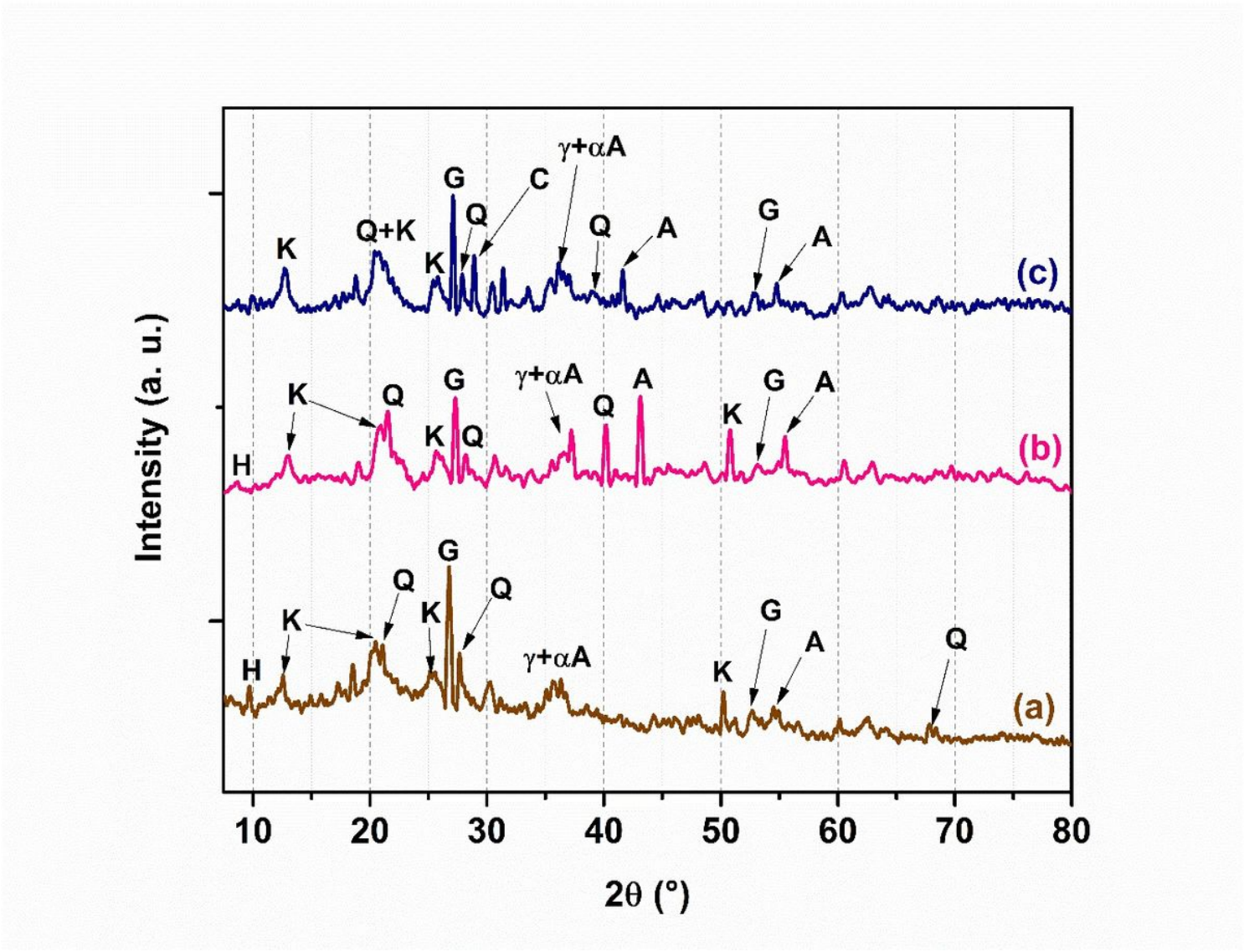

Figure 4

PXRD patterns for the synthesized biochars (a) BC3, (b) BC5 and (c) BC7. The symbols mean: H = halloysite, K = kaolinite, Q = quartz, A = alumina, and G = graphite.

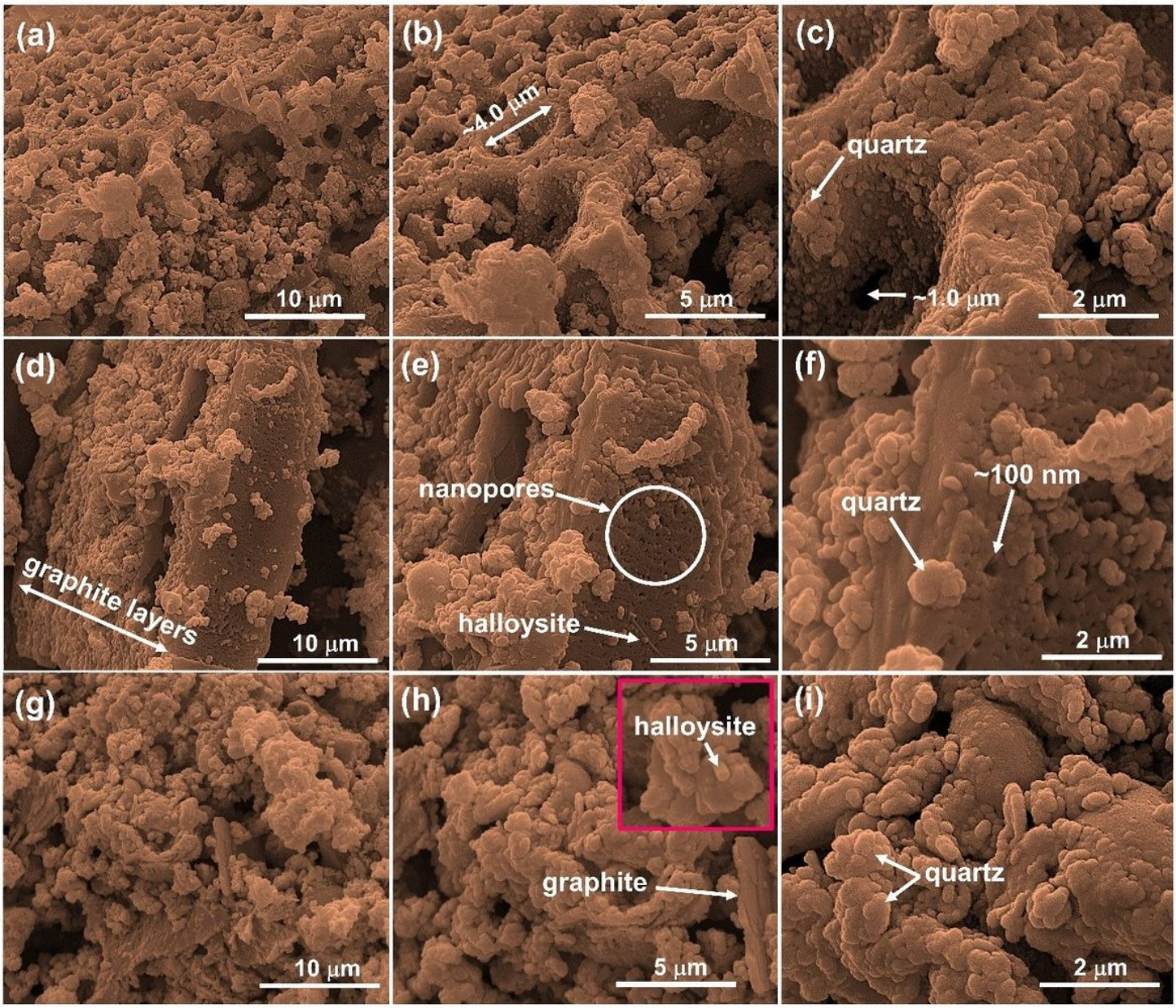

Figure 5

SEM images obtained for the synthesized biochars (a-c) BC3, (d-f) BC5, and (g-i) BC7.

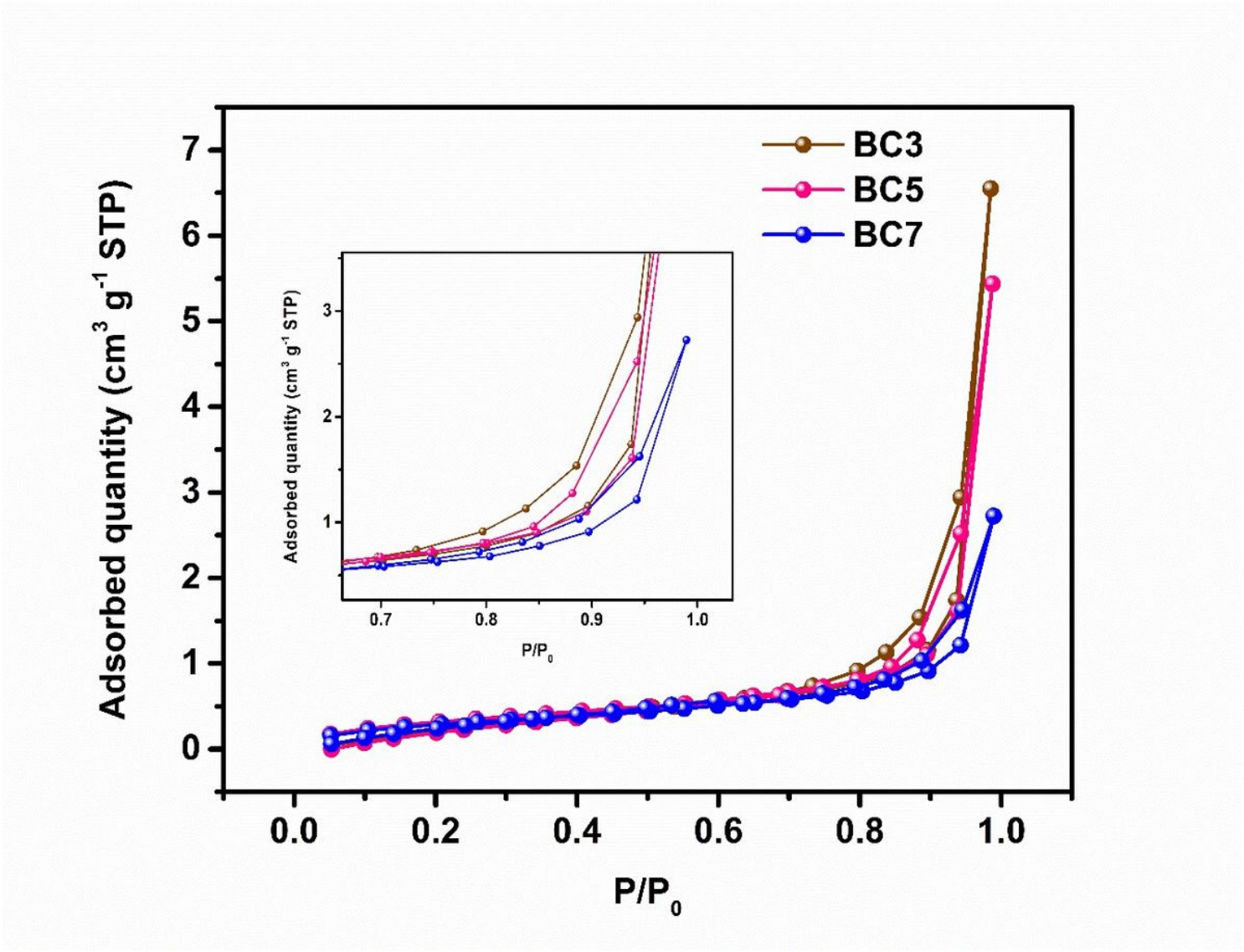

Figure 6

N2 adsorption-desorption isotherms obtained for the synthesized biochars.

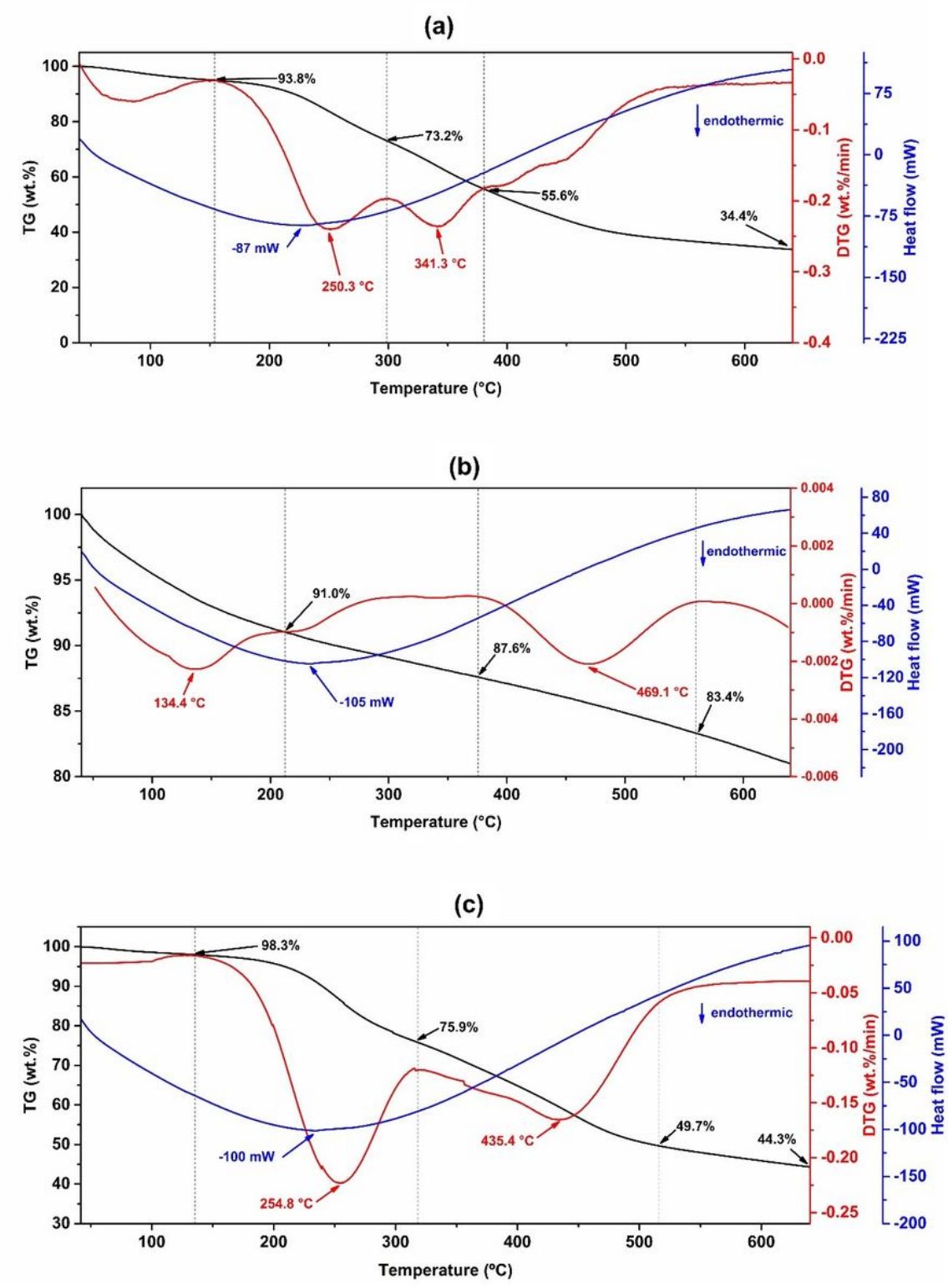

Figure 7

TGA results obtained for (a) BC3, (b) BC5 and (c) BC7.

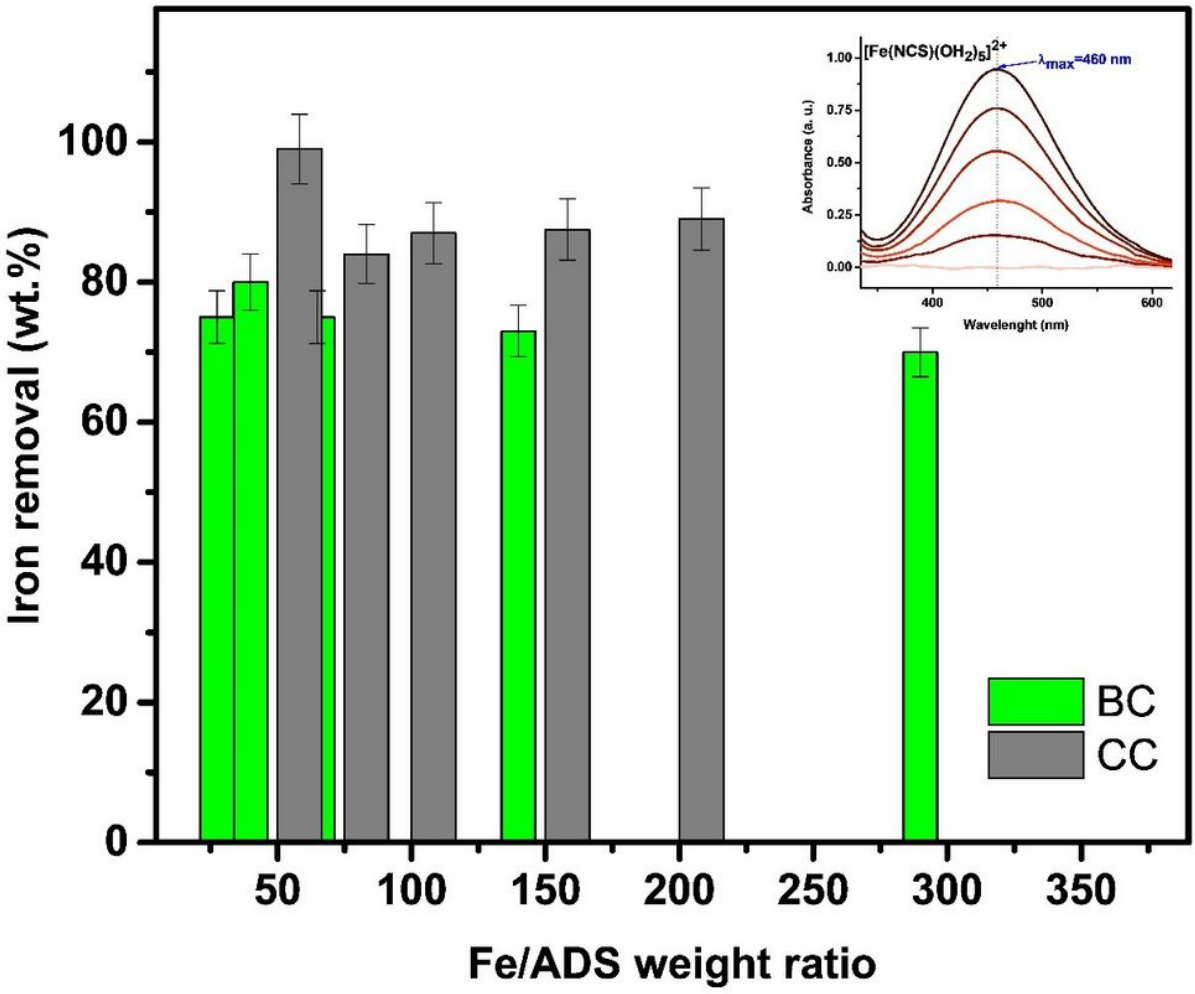

Figure 8

Adsorption of iron(III) on BC5 and CAC. The experimental error was estimated as an average of 5%.

Supplementary Files

This is a list of supplementary files associated with this preprint. Click to download.

- Graphicalabstract.docx